Stress Dependence of Sapphire Cathodoluminescence from Optically Active Oxygen Defects as a Function of Crystallographic Orientation

Maria Chiara Munisso, Wenliang Zhu, Andrea Leto, and Giuseppe Pezzotti*

Ceramic Physics Laboratory & Research Institute for Nanoscience, RIN, Kyoto Institute of Technology, Sakyo-ku, Matsugasaki, 606-8585 Kyoto, Japan

Received: December 13, 2006; In Final Form: March 2, 2007

The cathodoluminescence (CL) spectrum of the synthetic sapphire single crystal has been studied with respect to the different crystallographic planes of the crystal in order to describe the tensorial stress dependence of the band related to oxygen defects. Experiments provide the link between CL spectral shift and stress, which is referred to as the piezo-spectroscopic (PS) relationship. Using the biaxial stress field developed at the tip of cracks generated from the corners of a Vickers indentation, we clearly detected stress dependence for the cumulative band arising from the F^+-center transition of optically active oxygen vacancies. The matrix of PS coefficients along different crystallographic axes of single-crystal sapphire could be precisely determined. The shallow nature of the electron probe may enable the characterization of surface stress fields with a spatial resolution that may not be easily available by conventional laser probes. The PS calibration results collected on oxygen-defect bands allow the direct determination of unknown surface residual stress fields stored in sapphire substrates for electronics applications.

Introduction

Synthetic sapphire single crystals are available in the crystallographic form of corundum, also known as alpha-alumina (α-Al_2O_3). The combination of favorable chemical, electrical, mechanical, optical, surface, thermal, and durability properties makes sapphire a preferred material for high-performance systems and component design. Nowadays, single-crystal sapphire plays an increasingly important role as a material for high-reliability devices, because of its excellent mechanical characteristics, chemical stability, and light transmission. It is an ideal substrate for epitaxial deposition of GaN and other thin-film materials for use in the manufacture of bright blue and green light emitting diodes.[1] Applications of this material in a hostile environment, such as in the presence of radiations, high temperature, or external electromagnetic fields, has constituted the driving force for understanding the effects related to electronic and bounding structure, in particular, in the presence of impurities and defects[2,3] and of residual stress fields.[4,5]

In the Al_2O_3 lattice, a part per million level of Cr_2O_3 is commonly present (Cr^{3+} is a natural substitutional metal ion for Al^{3+}).[2,6] As a consequence of relaxation from the first excited state of Cr^{3+} ion to its ground state, two sharp luminescence bands, usually referred to as the R_1/R_2 doublet, appear at room temperature in the red visible range, located at 694.3 nm (1.786 eV) and 692.9 nm (1.789 eV), respectively. In the presence of lattice defects, extra luminescence emissions can be observed in the ultra-violet (UV) region upon highly energetic excitation. Lee and Crawford[7] first proposed that the additional UV luminescence in sapphire is related to oxygen vacancies. In the general case, the observed UV spectrum is also a doublet and can be deconvoluted into two distinct sub-band components: an F^+-center band, located at around 325 nm (3.8 eV), and a less intense F-center band, located at around 415 nm (3.0 eV).[8] The F^+- and F-center emissions were related to a single oxygen vacancy trapping one or two electrons, respectively.[9,10] After the trapped electrons have been highly energetically excited, a de-excitation process takes place, which splits into several individual transitions. The final transition of the electron(s) to the ground state leads to the above-mentioned emission of a photon for F^+ and F centers, respectively. However, Draeger and Summers[11] showed that the intensity of the F emission relative to that of F^+ is low for electron-irradiated α-Al_2O_3.

Residual stress states stored in Al_2O_3-based materials[5] have been extensively measured by exploiting the piezo-spectroscopic (PS) behavior of its photostimulated chromophoric luminescence emission (i.e., the R_1/R_2 doublet).[5,6,12] However, given the high transparency of sapphire, when a laser beam probes the ruby lines of a sapphire single crystal, it cannot easily be confined to regions shallower than tens of microns even by adopting a highly confocal probe configuration.[13] Exploitation of selected Raman bands from the corundum structure has been suggested for improving the spatial resolution of the laser probe.[14,15] Although this practice may enable one to reach a spatial resolution close to 1 μm, a lower limit for laser probe size is unavoidably confined to the micron scale, because of limitations dictated by the laser wavelength and by the optical efficiency of the laser probe. From the point of view of spatial resolution, a low-energy electron probe can in principle lead to a spatial resolution more than 2 orders of magnitude higher than that achieved by photoluminescence assessments. This may prove particularly useful when one needs to probe the very surface of materials or devices. When electrons are used for exciting the luminescence spectrum of undoped sapphire crystals, the efficiency of the chromophoric emission is quite low, while the UV emission from oxygen defects is enhanced. In a previous paper,[16] we have shown the linear link between wavelength shift of the F^+-defect band from c-plane sapphire and externally applied stress. Building upon this finding, we present in this paper a complete set of PS calibrations for the oxygen-related defect band collected from all of the crystallographic planes of sapphire. This approach enables the systematic determination of all of the components of the PS tensor, thus exploring the feasibility of precise stress assessments along different crystallographic orientations.

* Corresponding author. E-mail: pezzotti@kit.ac.jp.

Stress Dependence of Sapphire Cathodoluminescence

J. Phys. Chem. A, Vol. 111, No. 18, 2007 **3527**

Experimental Procedures

Four sapphire single-crystal samples were analyzed, which were oriented on their $(1\bar{1}02)$, $(10\bar{1}0)$, (0001), and $(11\bar{2}0)$ planes (corresponding and henceforth referred to as the *R*, *a*, *c*, and *m* planes, respectively). All samples were obtained from a commercially available crystal (Kyocera, Co., Tokyo, Japan). Prior to spectroscopic characterization, the samples were polished with fine diamond paste (0.1 μm) and annealed, in order to minimize the effect of residual stresses due to crystal growth and subsequent surface machining.

Cathodoluminescence (CL) spectra were collected by means of a field-emission gun scanning electron microscope (FEG-SEM, SE-4300, Hitachi Co., Tokyo, Japan) equipped with a CL device, consisting of an ellipsoidal mirror and a bundle of optical fibers to collect and focus the electro-stimulated luminescence emission into a highly spectrally resolved monochromator (Triax 320, Jobin-Yvon/Horiba Group, Tokyo, Japan). A 600 gr/mm grating and a liquid-nitrogen-cooled 1024 × 256 pixels charge coupled device (CCD) was used to analyze the CL emission of the material.

A diamond-tip Vickers indenter (AVK-C1, Akashi Co., Tokyo, Japan) was used to print controlled Vickers indentations on the crystal surface with an applied load of 0.1 kgf. The residual stress field stored at the tip of microcracks, propagating from the corners of the indentation print, were quantitatively evaluated using the crack opening displacement (COD) method and were used for the PS calibrations.

Theoretical Background

A. PS Tensorial Formalism in the Corundum Structure. According to the PS effect, the stress state in a thermally homogeneous crystal can be related to the wavelength shift, $\Delta\lambda$, of a given luminescence band with respect to its unstressed state. A tensorial formalism has been proposed by Grabner[17] for describing the PS effect in the case of a chromophoric impurity embedded in the crystal lattice. We shall assume in the remainder of this paper that Grabner's formalism holds validity for a point defect in general, irrespective of the defect being a substitutional atom or a vacancy. Grabner's equation can then be generalized to the optical activity of an oxygen vacancy as follows:

$$\Delta\lambda = \begin{pmatrix} \Pi_{11} & \Pi_{12} & \Pi_{13} \\ \Pi_{21} & \Pi_{22} & \Pi_{23} \\ \Pi_{31} & \Pi_{32} & \Pi_{33} \end{pmatrix} \cdot \begin{pmatrix} \sigma_{11} & \sigma_{12} & \sigma_{13} \\ \sigma_{21} & \sigma_{22} & \sigma_{23} \\ \sigma_{31} & \sigma_{32} & \sigma_{33} \end{pmatrix}^T = \Pi_{ij}\sigma_{ij} =$$

$$\begin{pmatrix} \Pi_{11} & 0 & 0 \\ 0 & \Pi_{22} & 0 \\ 0 & 0 & \Pi_{33} \end{pmatrix} \cdot \begin{pmatrix} \sigma_{11}^* & 0 & 0 \\ 0 & \sigma_{22}^* & 0 \\ 0 & 0 & \sigma_{33}^* \end{pmatrix}^T = \Pi_{ii}\sigma_{ii}^* \quad (1)$$

where $i, j = 1, 2, 3 = x, y, z$; $\Delta\lambda = \lambda - \lambda_0$ is the wavelength shift observed with respect to an unstressed wavelength, λ_0; the repetitive index notation is applied to a general stress state, σ_{ij}; and Π_{ij} is the second-rank tensor of PS coefficients. The asterisk denotes the choice for the stress tensor of a set of Cartesian axes co-incident with the principal stress directions. The PS tensor is always referred to the crystallographic axes of the material.[17] For the corundum structure of sapphire, crystallographic symmetry suggests[5] that $\Pi_{11} = \Pi_{22} \neq \Pi_{33}$ (with the indexes 1, 2, and 3 referring to the crystallographic directions *a*, *m*, and *c*, respectively).

In the case of a general bi-axial stress state, σ_{ii}^*, applied in the basal crystallographic (*c*) plane of the sapphire sample, eq 1 simply reduces to a scalar equation as follows:

$$\Delta\lambda = \Pi_{11}\sigma_{11}^* + \Pi_{22}\sigma_{22}^* \equiv \Pi \cdot \sigma_{ii}^* \quad (2)$$

where $\Pi = \Pi_{11} = \Pi_{22}$ and $\sigma_{ii}^* = \sigma_{11}^* + \sigma_{22}^*$ is the trace of the principal stress tensor. In other words, a measurement of spectral shift gives direct access to the trace stress tensor. On the other hand, in any crystallographic plane different from the basal plane, a scalar equation similar to eq 2 can be obtained only in the case of an equi-biaxial stress state. For example, for the *a* plane:

$$\Delta\lambda = \Pi_{22}\sigma_{22}^* + \Pi_{33}\sigma_{33}^* \equiv \Pi \cdot \sigma_{ii}^* \quad (3)$$

with $\sigma_{22}^* = \sigma_{33}^*$ and $\Pi = (\Pi_{22} + \Pi_{33})/2$. It follows that the trace of an equi-biaxial residual stress tensor locally stored in any crystallographic plane of sapphire can be measured according to eqs 2 or 3, provided that the PS coefficient, Π, can be evaluated by introducing into the material a known equi-biaxial stress state.

B. Calibration Method Using Crack-Tip Stress Field. The local residual stress induced ahead of an indentation crack can be described by fracture mechanics equations as a function of polar coordinates, (r,θ), with origin at the crack tip:

$$\begin{pmatrix} \sigma_{11} \\ \sigma_{22} \\ \tau_{12} \end{pmatrix} = \frac{K_I}{\sqrt{2\pi r}} \begin{pmatrix} \cos\dfrac{\theta}{2}\left[1 - \sin\dfrac{\theta}{2}\sin\dfrac{3\theta}{2}\right] \\ \cos\dfrac{\theta}{2}\left[1 + \sin\dfrac{\theta}{2}\sin\dfrac{3\theta}{2}\right] \\ \sin\dfrac{\theta}{2}\cos\dfrac{\theta}{2}\cos\dfrac{3\theta}{2} \end{pmatrix} \quad (4)$$

where K_I is the crack-tip stress intensity factor. Along a line straight ahead of the crack path ($\theta = 0$), the stress field is equibiaxial and eq 4 reduces to:

$$(\sigma_{11},\sigma_{22}) \equiv (\sigma_{11}^*,\sigma_{22}^*) = \left(\frac{K_I}{\sqrt{2\pi r}}, \frac{K_I}{\sqrt{2\pi r}}\right) \quad (5)$$

A PS calibration will then consist in the determination of the spectral shift, $\Delta\lambda$, (taken with respect to the unstressed spectral position) of a selected CL band, when a known tensorial stress state is applied to the material or, in other words, in the determination of the PS coefficient, Π, of the material (i.e., as given by eqs 2 and 3). However, in order to apply eq 5 to a PS calibration, an additional procedure is required for assessing the K_I value. This latter parameter can be obtained by a preliminary measurement of the COD, $U(x)$, from high-resolution FEG-SEM images.[18] A detailed explanation of this procedure has been given elsewhere,[19] and we briefly report here about the salient features of this characterization. For a half-penny shaped crack configuration, K_I and $U(x)$ can be related through the following equation:[20]

$$U(x) = \frac{4K_I}{\pi E'} Y\left(\frac{x}{a}\right) \quad (6)$$

where the weight function $Y(x/a)$ for an indentation crack is given by:

$$Y\left(\frac{x}{a}\right) = \sqrt{b}\left[A\left(\frac{x}{a}\right)^{1/2} + B\left(\frac{x}{a}\right)^{3/2} + C\left(\frac{x}{a}\right)^{5/2}\right] \quad (7)$$

$$A = \left(\frac{\pi a}{2b}\right)^{1/2} \quad (8)$$

$$B \cong 0.011 + 1.8197 \ln\left(\frac{a}{b}\right) \quad (9)$$

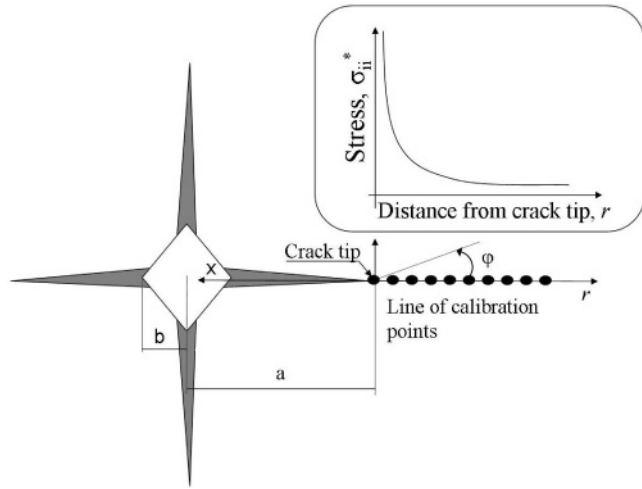$$C \cong -0.6513 + 2.121 \ln\left(\frac{a}{b}\right) \quad (10)$$

Figure 1. Schematic of an indentation print with the salient parameters involved with the PS characterization. A qualitative plot of the stress field developed ahead of the tip of a crack propagated from an indentation corner of the print is shown in inset.

where x is an abscissa taken along the crack path (with an opposite direction to crack propagation, i.e., $x = -r$), a is the distance between the crack tip and the center of the indentation print, b is half the diagonal of the indentation print, and $E' = E/(1 - \nu^2)$ is the plane stress Young's modulus of the material (with E being Young's modulus and ν being Poisson's ratio of the crystal in the plane of crack propagation). Figure 1 shows a schematic of the indentation print, a qualitative plot of the stress field developed ahead of the tip of a crack propagated from a corner of the print (in inset), and the salient parameters involved with the characterization. Equations 2 (or 3) and 5−7 can be rearranged to obtain the local stress ahead of the crack tip in any crystallographic plane of sapphire as follows:

$$\frac{\sigma_{ii}^*}{2} = \frac{\pi E' U(x)}{4\sqrt{2\pi r} \cdot \sqrt{b}} \cdot \left[A\left(\frac{x}{a}\right)^{1/2} + B\left(\frac{x}{a}\right)^{3/2} + C\left(\frac{x}{a}\right)^{5/2} \right]^{-1} = \frac{\Delta\lambda}{2\Pi} \quad (11)$$

CL spectra can be collected ahead of the crack tip by a line scan, and from the slope of a plot $\Delta\lambda$ versus σ_{ii}^*, the PS coefficient, Π, for any crystallographic plane can be determined. Note that the validity of eq 11 can be strongly hindered by the finite volume of the electron probe, because of the highly steep stress gradient developed at the crack tip. Therefore, for a correct evaluation of the Π value, the effect of the size of the electron probe on the monitored stress magnitude should be taken into due consideration.

C. Size of and In-Plane Luminescence Distribution in the Electron Probe. The experimental size of the selected probe depends on the nature of the interaction between solid target and electron beam and may lead to considerable complications in interpreting the collected spectra in terms of stress, especially in the presence of highly anisotropic property distributions. To counteract the problems related to finite probe size, a probe response function (PRF), namely, the luminescence distribution function developed within the probe, can be experimentally retrieved from high-resolution line scans across a straight and atomically sharp interface between the studied crystal and a different material. Assuming that each point in space (x,y,z) gives rise to a (local) intensity contribution to the electron stimulated spectrum of a given morphology, we find that the observed spectrum will depend on the energy distribution of the incident electrons along their diffusional path within the material. When an incident beam with acceleration voltage, V, is focused at an
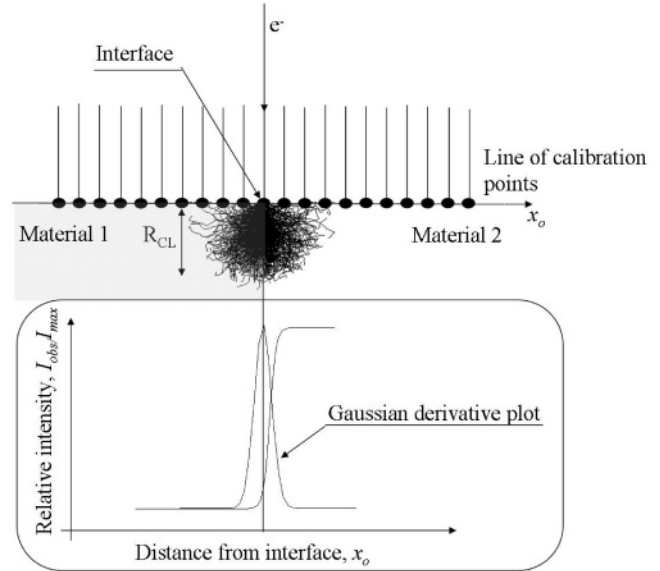

Figure 2. Schematic of a PRF calibration procedure across a sharp interface between different materials. The inset shows a plot of intensity variation as a function of electron beam position and its derivative.

arbitrary point (x_0, y_0, z_0), the energy distribution can be represented by the PRF, $G(x,y,z;x_0,y_0,z_0;V)$ and the observable CL spectrum can be expressed according to the following triple integral:

$$I_{\text{obs}}(\lambda) = \int_{-\infty}^{+\infty} \int_{-\infty}^{+\infty} \int_{0}^{+\infty} I(x,y,z) \, G(x,y,z;x_0,y_0,z_0;V) \, dx \, dy \, dz \quad (12)$$

where $I_{\text{obs}}(\lambda)$ is the observed CL spectrum and $I(x,y,z)$ is the intrinsic amount of CL emission generated at each location within the probe. The in-plane PRF is attentioned in this study because the stress variation along the variable abscissas, z and z_0, in the in-depth direction for an indentation crack of median configuration can be ignored. A proof for this assertion is given in ref 13. In the case of a line scan across an interface, as the probe is translated, for example, along the x axis, the maximum (at $\lambda = \lambda_{\text{p}}$) of the collected CL intensity, $I_{\text{obs}}(\lambda_{\text{p}})$, maps the probe response and can be expressed by a simplification of eq 12 as follows:

$$I_{\text{obs}}(\lambda_{\text{p}}) \propto \int_{0}^{+\infty} \int_{-\infty}^{+\infty} G(x,y;x_0,y_0;V) \, dx \, dy \quad (13)$$

where the abscissa $x \equiv x_0$ is taken with origin at the interface between the two materials. The intensity variation of the selected CL band can be collected as a function of distance, x_0, between the interface and the location of the center of the electron beam. Figure 2 shows a schematic of PRF calibration procedure across a sharp interface between different materials and, in the inset, shows a plot of intensity variation as a function of the electron beam position. Note that, when scanning across the interface from different directions, there might be asymmetry in the experimentally retrieved CL intensity curves, because of the property (i.e., electron-diffusion length) difference between the two adjacent materials. However, the probe-related parameters can be generally derived from the best fitting of the normalized experimental intensities at selected locations within the investigated material. The differential contribution of each portion of volume of the luminescent probe (i.e., the intensity variation as a function of distance between the interface and the irradiated center) can then be obtained from plotting the first derivative

Stress Dependence of Sapphire Cathodoluminescence

J. Phys. Chem. A, Vol. 111, No. 18, 2007 **3529**

of the normalized CL intensity, $I_{obs}(\lambda_p)$, as a function of the abscissa, x_0 (cf. derivative plot in the inset of Figure 2). Derivative plots can be generally represented according to a Gaussian equation as follows:

$$G(x,y,x_0,y_0,V) = C_1 \exp \frac{-(x-x_0)^2}{C_2 V^n} \times \exp \frac{-(y-y_0)^2}{C_2 V^n} \quad (14)$$

where the constant C_1 is a function of V but can be taken = 1, after normalizing the plots to the respective CL intensity maxima; C_2 and n can then be determined according to a least-square fitting procedure of the experimental curves. Note that the choice of the same constant C_2 along x and y directions is an approximation because it implies no preferential electron diffusion, light scatter, or both regarding the orientation of the crystal. It should be noted that the empirical Gaussian function given in eq 14 holds validity only at relatively low acceleration voltages, while, at high acceleration voltages, the morphology of the function might be altered by the contribution of multiple scattering of the electrons.

When the luminescent probe is taken to be symmetric in any given xy plane, its size, R_{CL}, can be defined in first approximation according to the following equation:

$$\frac{\int_{x_0-R_{CL}}^{x_0+R_{CL}} G(x,x_0,V)\,dx}{\int_{-\infty}^{+\infty} G(x,x_0,V)\,dx} = 0.9 \quad (15)$$

Note that the choice of the factor 0.9 in eq 15 is arbitrary, but it is based on the understanding that any intensity contributions <10% from remote parts of the electron probe will hardly affect the spectral location of the band maximum, according to which we shall assess the stress magnitude in the remainder of this paper.

The CL probe size can eventually be compared with the primary electron probe range, R_{el}, as a function of acceleration voltage, V. This latter parameter can be calculated according to the Kanaya−Okayama equation:[21]

$$2R_{el} = \frac{2.76 \times 10^{-2} \times A}{\rho Z^{0.889}} V^{1.67} \quad (16)$$

where ρ is the crystal density, A its atomic mass number, and Z its atomic number (3.98 g/cm^3, 101.94 g/mol, and 88, respectively, for a sapphire crystal). On the basis of the experimental knowledge of PRF, a two-dimensional probe deconvolution can be attempted to restore the collected stress data. We shall propose in the forthcoming section V a deconvolution procedure, which takes into account individual spectral contributions from different portions of the finite probe size according to the experimentally determined PRF.

Experimental Results

A. CL Spectrum from Optically Active Oxygen Defects. A typical CL spectrum in the UV region arising from oxygen-related point defects in a sapphire single crystal is shown in Figure 3a after normalization to its maximum intensity, I_{max}. The spectrum shown was taken on the c plane of the crystal (electron irradiation at 4 kV and 300 pA); however, no detectable morphological difference, except for the spectral intensity, was noticed for collection on different crystallographic planes, whose spectra are therefore omitted here. The effect of oxygen vacancies in ionic oxide crystals has been long known
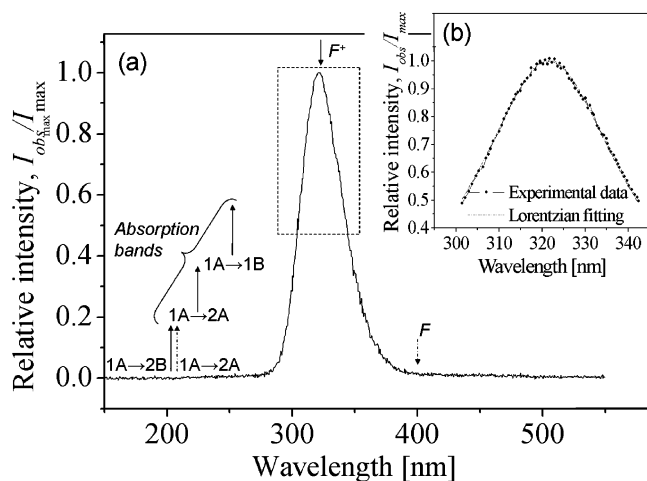

Figure 3. (a) CL spectrum of sapphire single crystal representing with its F^+ band the optical activity of oxygen vacancies; (b) high-intensity portion of the spectrum fitted to a Lorentzian curve.

by spectroscopists because it involves a clear coloration of the sample.[22] In particular, the spectrum shown in Figure 3a represents the optical activity of oxygen vacancies, also referred to as F^+ centers (where the letter "F" stands from the German word "farbe" meaning "color"). Removal of oxygen ions from the sapphire lattice can be either in the form of O or in the form of O$^-$, leading to the presence in the CL spectrum of two distinct bands, usually referred to as F and F^+ centers, respectively. In other words, two different patterns for the oxygen defects are possible in the sapphire lattice: (i) an F center, which contains two electrons trapped in the vacancy; and (ii) an F^+ center, which involves a single-trapped electron and represents a paramagnetic defect. The F centers involve an optical spectrum which is dominated by a single absorption band centered at 6.05 eV (i.e., corresponding to the $1A \rightarrow 2A$ transition). On the other hand, the F^+ center gives rise to two different absorption bands (located at about 4.8 and 5.4 eV, respectively). Also, a third band has been revealed by time-resolved spectroscopy.[9] This band is centered at 5.95 eV, and thus partially overlaps the F center absorption band. The three F^+-center-related bands have been assigned to $1A \rightarrow 2B$, $1A \rightarrow 2A$, and $1A \rightarrow 2B$ transitions, respectively.[23] As far as emission is concerned, a singlet luminescence band (located at 3.26 eV) has been reported for the F^+ center.[24] This corresponds to the CL spectrum actually observed in this study (cf. Figure 3a) at room temperature. It should be noted, however, that decay of excited F states has been reported to be a complex phenomenon which involves an $F \rightarrow F^+$ deactivation channel.[24] Furthermore, when the very surface of the sample is involved (which may be the case here by probing with a very shallow electron probe), more complex structures (e.g., those related to a single electron trapped and a neighboring H$^+$ center) have also been suggested to describe paramagnetic defects in ionic crystals. One can thus expect that surface structures contribute in a non-negligible amount to the spectral morphology observed here. In Figure 3a, we have labeled all of the electronic transitions related to the (absorption and emission) activity of oxygen vacancies, according to a scheme reported in the literature.[7−11,23,24] From a spectroscopic point of view, the observed CL spectrum appears to be asymmetric, thus, differing from standard Gaussian or Lorentzian curves. However, such an asymmetry was confined to the low-intensity portions of the band. When the high-intensity portion ($I/I_{max} > 0.5$) of the band was taken into consideration (cf. part of the F^+ band in the square area of Figure 3a), the obtained portion of the spectrum was substan-
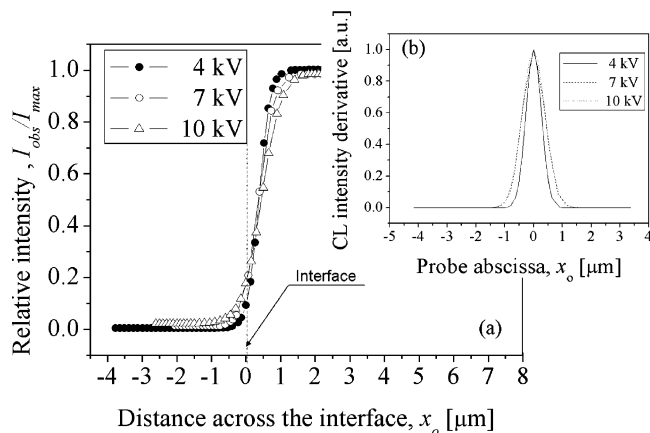
Figure 4. (a) CL relative intensity line scans at three different electron acceleration voltages (V = 4, 7, and 10 kV) across an interface between c plane sapphire and barium titanate film; (b) first derivative of the normalized CL intensity function in (a), representing the differential contribution of individual portions of volume in the luminescent probe.

tially symmetric and could be fitted to a high degree of precision ($R^2 > 0.999$) according to a Lorentzian curve, as also shown in Figure 3b. Changing the electron irradiation conditions led to slight changes in the morphology of the F^+ band; however, the recorded spectrum was quite stable at fixed irradiation conditions. By translating this notion in terms of PS assessments, it is found that the CL spectrum assumed as a standard stress-free reference should be rigorously collected under the same electron irradiation conditions adopted for screening stressed areas of the crystal. Despite the limitation of having a probe-dependent spectrum, the fitting procedure depicted in Figure 3b was found to be generally suitable for single-crystal sapphire, independent of the adopted electron irradiation conditions.

B. In-Plane PRF and Primary Electron Probe Range. The intensity change of the F^+ CL band was experimentally collected as a function of location of the electron beam, x_0 (or y_0), by scanning across a sharp interface. The results of CL intensity line scans (at three different electron acceleration voltages: V = 4, 7, and 10 kV) across an interface between c-plane sapphire and a barium titanate film are shown in Figure 4a. The differential contribution of each portion of volume of the luminescent probe (i.e., the first derivative of the normalized CL intensity function) was then obtained, as shown in Figure 4b). No significant difference was found for scanning along different crystallographic directions. The best fit to the experimental data collected at different voltages was obtained, according to eq 14, by selecting the probe-related parameters C_2 and n as 0.064 and 0.77, respectively. As can be seen from Figure 4a, the intensity of the CL signal emitted from the sapphire side of the bimaterial sample was not exactly located at the interface, because of preferential electron broadening from the barium titanate side. However, high symmetry was found in the derivative plot displayed in Figure 4b (i.e., the PRF for the F^+ band of sapphire). For the purpose of the present investigation, the PRF was thus intentionally translated with its center at the bimaterial interphase because no appreciable anisotropic electron broadening can be expected in measuring stress fields in bulk sapphire. Note also that the choice of the same constant C_2 along x_0 and y_0 directions implies no preferential orientation in the sapphire crystal regarding not only electron diffusion but also light emission scatter. A comparison between CL probe size and electron probe size can be made, for example, at V = 4 kV, by calculating these two parameters according to eqs 15 and 16, respectively. The values R_{CL} =
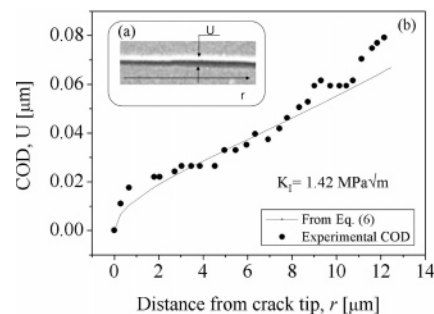

Figure 5. (a) High-resolution FEG-SEM image used for COD characterization of indentation cracks in sapphire; (b) typical COD plot for a c plane crack propagated along the a axis in sapphire.
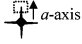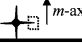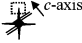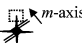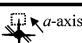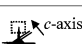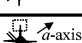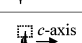
TABLE 1: K_I Values Retrieved from COD Plots, Indentation Parameters, and the Elastic Constants[26] for Different Crystallographic Planes of Sapphire

		indentation parameter				
plane	axis	a [μm]	b [μm]	K_I [MPa$\sqrt{m}$]	R^2	E' [GPa]
c	a	25.11	7.53	1.42	0.88	423
	m	27.82	9.7	1.94	0.85	
A	c	27.82	9.7	1.32	0.89	462
	m	27.96	8.55	1.89	0.94	
m	a	33.83	9.23	1.49	0.82	462
	c	33.97	10.39	1.35	0.89	
R	a	54.85	18.19	1.73	0.85	429
	c	41.44	7.72	1.94	0.93	

600 nm and R_{el} = 140 nm are found, suggesting a light diffusive contribution to the CL probe size in the highly transparent sapphire crystal. The experimental knowledge of PRF and probe size constitutes the basis for a deconvolution procedure to restore stress data collected in highly graded areas (e.g., at crack tip) from the effect of the finite size of the probe.

C. Crack-Tip Stress Intensity Factors for Different Crystallographic Planes. A Vickers indentation was used to generate a micrometer-sized squared print within selected crystallographic planes of sapphire. Cracks, which extended from the corners along the diagonal directions of the indentation print, developed a biaxial (tensile) stress field ahead of their tips. Such a residual stress field was precisely assessed by monitoring the COD of the crack from high-resolution SEM images (Figure 5a). The crack-tip stress intensity factor, K_I, of a median indentation crack propagated from the corner of an indentation print (cf. geometrical parameters in Figure 1) was quantitatively assessed according to eqs 6–10. A typical COD plot for a c-plane crack propagated along the a axis in sapphire is shown in Figure 5b. The stress intensity obtained from the COD plot was K_I = 1.42 MPa $\times$ m$^{1/2}$, according to a least-square fitting procedure (cf. Figure 5b) on the experimental data (with taking $E'f$ = 423 GPa).[25] Note that the detected K_I value may be close but not exactly represent the critical stress intensity factor, K_{Ic}, of the crystal; however, K_I = K_{Ic} does not represent a necessary condition for applying the indentation crack-tip stress field to a PS calibration.[26-29] Table 1 summarizes the K_I values (together with the indentation parameters and the elastic constants)[25] retrieved from COD plots on different crystallographic planes of sapphire. It should be noted that the crack morphology for indentation printed on different crystallographic planes and with corners oriented along different crystallographic axes was not always straightforward. Main cracks could be only propagated along cleavage directions and secondary cracks, as well as surface steps originated from dislocation gliding, appeared at locations different from print corners. In this study,

Stress Dependence of Sapphire Cathodoluminescence

J. Phys. Chem. A, Vol. 111, No. 18, 2007 **3531**

TABLE 2: Π Values Retrieved for All Crystallographic Planes of Sapphire along Different Crystal Axes[a]

Plane	Axis	2Π [nm/GPa]	ΔΠ [nm/GPa]	R^2	Crack morphology
c	a	0.72	± 0.07	0.88	a-axis
	m	0.77	± 0.08	0.86	m-axis
a	c	1.6	± 0.06	0.89	c-axis
	m	0.58	± 0.09	0.70	m-axis
m	a	1.85	± 0.08	0.86	a-axis
	c	1.93	± 0.02	0.96	c-axis
R	a	1.07	± 0.02	0.96	a-axis
	c	0.87	± 0.07	0.88	c-axis

[a] The error involved with the PS measurement and the deviation from a linear PS plot rationalized in terms of the correlation factor R^2 are also listed. Schematics are also shown of the morphology obtained for indentations printed on different crystallographic planes. The broken-line squares represent the crack-tip areas investigated. Straight lines, besides cracks, represent the gliding planes.

we made an effort in rotating the crystal surface with respect to the indenter in order to reliably generate main cracks from corner prints on different crystallographic planes and used only those cracks for the PS characterization. Detailed schematics of the morphology obtained for indentations printed on different crystallographic planes are given in Table 2.

D. Crack-Tip Spectral Shift Profiles in Different Crystallographic Planes. Several line scans (with a sampling step of 40 nm) were carried out along the propagation direction of indentation cracks in different crystallographic planes at the fixed voltage of 4 kV. We monitored the wavelength at maximum, λ_p, of the F^+ CL band (after Lorentzian fitting). A negligible variation in position and morphology of the F^+ band was observed in a 1×1 μm map scans (10×10 data points) collected at random locations of the crystal plane far away from the indentation print. While this experimental evidence confirms the homogeneous luminescence behavior of sapphire upon electron irradiation under the present electron probe conditions, it also shows that the investigated crystal surfaces contained a negligible amount of surface residual stress. According to this understanding, a "stress-free" reference wavelength, λ_0, could be retrieved from average spectra collected (under the same irradiation conditions) at a random location far away from the crack path. Typical spectral band-shift profiles obtained from scans on cracks propagated in different crystal planes along different axes are shown in Figures 6a–d (for a, m, R, and c plane, respectively). The crack-tip location was located in first approximation from the SEM micrograph (with an error <50 nm). Eventually the location was refined according to an extrapolation of the COD profile. As a general trend, the maximum of the band-shift plot was not exactly located in correspondence of the crack tip but slightly ahead of it. This was due to the finite size of the probe, whose effect will be discussed in the next section. Two additional features could be noticed in the experimental line scans: (i) in addition to a maximum in correspondence of the crack tip, another maximum of lower intensity was systematically found in a region just

behind the crack tip. This is due to the crack not being exactly at criticality and arises from the equilibrium stress field developed in this micromechanical situation around the crack tip.[30] Since this study is mainly concerned with the stress distribution ahead of the crack tip and crack criticality, as discussed above, is not a necessary condition for PS calibration, we shall not consider here further this phenomenon. Another feature is (ii) regions of the F^+-band shift profiles shown in Figure 6 ahead of the crack tip may not necessary coincide with cracks propagated along different crystallographic axes, although they will converge far away from the crack tip to the same stress-free wavelength. The studied cracks displayed different length when propagated along different crystallographic axes, and short cracks where still embedded into the residual stress zone developed around the indentation print.[30]

Attempts to improve the spatial resolution of the crack-tip spectral assessments by reducing the acceleration voltage of the electron beam below 4 kV failed because of the low efficiency of the CL emission. Note that, throughout the experiments, acquisition times as short as 1 s were adopted in order to avoid heating up the sample surface, while lowering *V* at <4 kV would require acquisition times more than 1 order of magnitude longer for the collection of spectra suitable for fitting.

Discussion

A. PS Coefficients for Different Crystallographic Planes of Sapphire. Using the experimentally measured PRF, $G(x,x_0,V)$, in Figure 4b and the experimental wavelength shift profiles, $\Delta\lambda_p$, collected ahead of the crack tip (Figure 6), we find it is possible to quantitatively assess the PS coefficient for different crystallographic planes of the sapphire crystal, according to eq 11. However, because of scattering of both electrons and photons in the crystal, the probe has a finite volume, and underestimation of the calculated PS coefficient may arise when the PS plots are made as a function of the theoretical crack-tip stress, σ_{ii}^* (calculated according to eq 4). Probe bias involved with the finite probe size can be avoided by considering that the observed wavelength shift actually occurs according to the stress magnitude, $\langle\sigma_{ii}^*\rangle$, convoluted over the finite volume of the electron probe. This latter stress value can be calculated at any location of the electron probe, x_0. The wavelength shift (with respect to an unstressed location) collected in the probe volume represents a convolution of the crack-tip stress field and can be expressed by

$$\overline{\Delta\lambda}(x_0,y_0;V) =$$

$$\frac{\int_{-\infty}^{+\infty}\int_{-\infty}^{+\infty} G(x,x_0,y,y_0;V) \times \Delta\lambda(x,y)\, dx\, dy}{\int_{-\infty}^{+\infty}\int_{-\infty}^{+\infty} G(x,x_0,y,y_0;V)\, dx\, dy} =$$

$$2\Pi K_I \frac{\int_0^{+\infty}\int_{-\pi}^{+\pi} \frac{r}{\sqrt{2\pi r}}\cos\frac{\theta}{2} \times \exp\left(-\frac{r^2+x_0^2}{C_2 V^n}\right) \times \exp\left(\frac{2rx_0\cos\theta}{C_2 V^n}\right) dr\, d\theta}{\int_0^{+\infty}\int_{-\pi}^{+\pi} r\exp\left(-\frac{r^2+x_0^2-2rx_0\cos\theta}{C_2 V^n}\right) dr\, d\theta} =$$
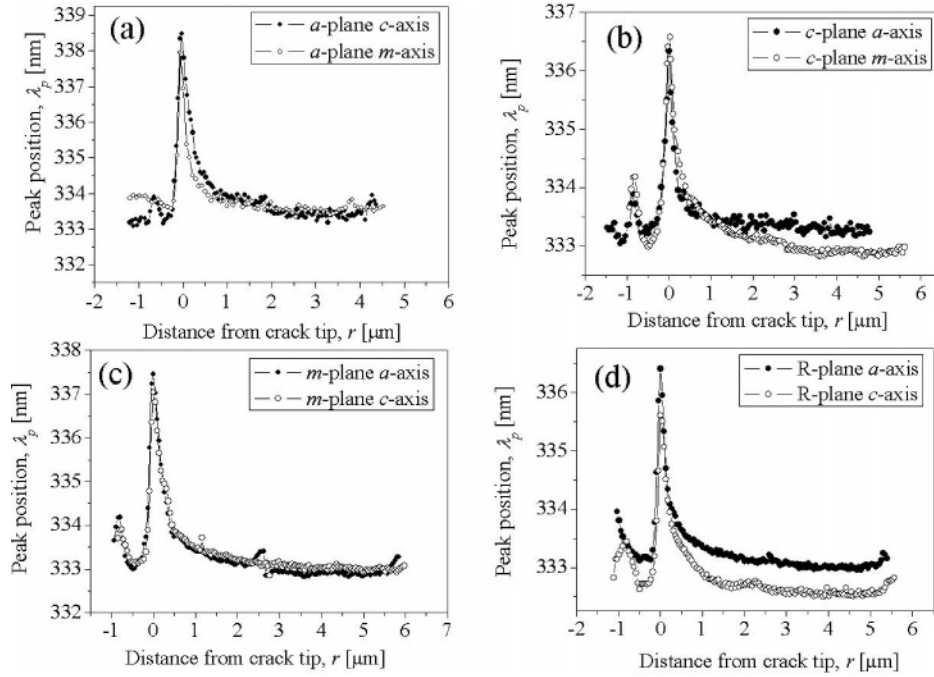
$$2\Pi\bar{\sigma}(x_0,0,0) \quad (17)$$

Figure 6. Typical spectral band-shift profiles as obtained from scans on cracks propagated in different crystal planes along different axes for *a*, *m*, *R*, and *c* plane (in a–d, respectively).
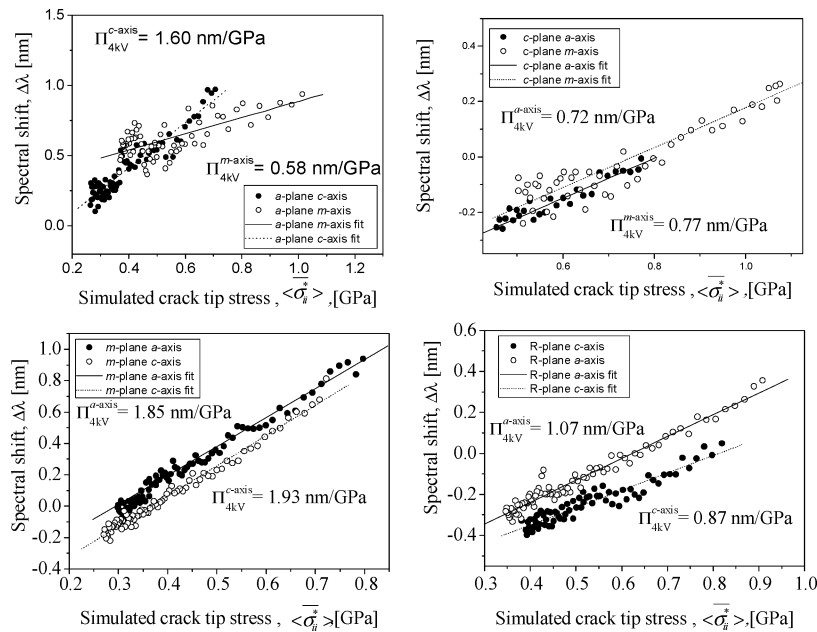

Figure 7. Typical PS plots of $\overline{\Delta\lambda}$ vs $\langle \overline{\sigma_{ii}^*} \rangle$ in a–d for *a*, *m*, *R*, and *c* plane, respectively.

where $\bar{\sigma}(x_0,0,0)$ is the convoluted (equi-biaxial) stress value at any location $P \equiv (x_0,0,0)$ ahead of crack tip. Note that the stress averaging effect along the in-depth direction has been neglected because the probe size was more than 2 orders of magnitude smaller than the crack depth. A complete discussion about electron probe convolution in highly graded stress fields has been given elsewhere.[27] The results of a numerical integration, according to eq 17, lead to a plot of $\overline{\Delta\lambda}$ versus $\langle \overline{\sigma_{ii}^*} \rangle$. In other words, the procedure of convoluting the stress magnitude developed into the electron probe enables one to retrieve the actual magnitude of the PS coefficient. The magnitude of this "true" Π value may be closer to Π values retrieved by using low-voltage probes without adopting any probe deconvolution procedure. However, in the case of highly transparent materials,

averaging the crack-tip stress field over the finite dimension of the probe may lead to underestimation of the Π value by about 15%.[27] Typical PS plots of $\overline{\Delta\lambda}$ versus $\langle \sigma_{ii}^* \rangle$ are shown in Figure 7a–d for *a*, *m*, *R*, and *c* plane, respectively. Following the above convolution procedure, "true" Π values were retrieved for all crystallographic planes of sapphire along different crystal axes, as summarized in Table 2. In the table, the error involved with the PS measurement is also shown, and the deviation from a linear PS plot is rationalized in terms of the correlation factor R^2. In support of the reliability of the present crack-tip PS characterization, it should be noted that the value found in this study for the PS coefficient for the *c* plane of sapphire was consistent with the PS value found for the same sample by the ball-on-ring calibration method.[16]

Stress Dependence of Sapphire Cathodoluminescence

J. Phys. Chem. A, Vol. 111, No. 18, 2007 **3533**

B. Technological Significance of CL/PS Calibration of Sapphire and Future Challenges. Sapphire is extensively used as a substrate for the growth of clusters and molecules. The *a* plane has been found to enable complexity and diversity in the formation of simple binary oxide compound structures on its surface[31−33] and provides a uniform dielectric constant and high insulation for hybrid microelectronic applications;[34] in particular, the *c* plane is used as a substrate to grow III−V and II−VI compounds such as GaN for blue laser diodes, while *R*-plane substrates are used for the hetero-epitaxial deposition of silicon for microelectronic integrated circuit applications.[34] Many of these applications are influenced by the residual stress fields stored on the surface of the sapphire crystal. In particular, the crystallographic quality of thin films grown on sapphire substrates as well as the structural reliability of those films strongly depends on the residual stress field stored in the first few atomic layers from the crystal surface. In this context, the electron probe may offer the shallowness and the scanning flexibility required for an accurate residual stress measurement on the crystal surface. Data in Table 2 provide a set of calibration values that may allow the quantitative evaluation of unknown residual stress fields stored on the surface of various crystalline planes of sapphire by monitoring its CL emission in a conventional SEM under a controlled electron irradiation. Future studies are required to relate the PS effect detected in the different crystallographic planes of sapphire through semiempirical rules obtained from ab initio relationships between the atomic structure of the defected lattice and the related luminescence emission. Finally, it should be noted that the effect of trace aliovalent impurities in sapphire may affect the CL spectrum observed from vacancy centers. We have observed, in particular, that increasing the amount of Cr^{3+} in sapphire (i.e., in ruby crystals) enhances the ruby doublet emission but strongly lowers the efficiency of CL emission from F and F^+ centers. In other words, surface stress fields in ruby crystals are hardly detectable by PS characterizations on oxygen defect luminescence.

Conclusion

We carried out CL experiments in order to assess the possibility of using the optical activity of oxygen-related defects as a surface residual stress sensor in sapphire single crystal. In all of the crystallographic planes of the crystal, clear stress sensitivity was found for the F^+ band related to a single electron trapped in a vacancy. This stress sensor possesses much higher spectral efficiency than the more conventional ruby doublet, when the luminescence is excited with a highly energetic beam. Using the residual stress field located at the tip of cracks generated by a Vickers indentation, we found that it was possible to retrieve a linear relationship between residual stress magnitude and peak shift, namely, a PS calibration line. Influence of CL probe size on the detected wavelength in the presence of a highly

graded stress field was taken into account by a stress convolution procedure, and precise values of PS coefficients could be collected as a function of the crystallographic orientation of sapphire. The present set of calibration data may thus allow for the quantitative assessment of unknown surface stress fields in sapphire crystals. Through engineering of the crystal surface stress state, improvement of processing procedures is possible, which can play an important role in several modern technological applications.

References and Notes

(1) Guo, J.; Ellis, E. D. E.; Lam, D. J. *Phys. Rev. B* **1992**, *45*, 13647.

(2) Shangda, X.; Changxin, G.; Libin, L.; Ellis, D. E. *Phys. Rev. B* **1987**, *35*, 7671.

(3) Lagerlöf, K. P. D.; Grimes, R. W. *Acta Mater.* **1998**, *46*, 5689.

(4) Ma, Q.; Clarke, D. R. *J. Am. Ceram. Soc.* **1990**, *77*, 298.

(5) Gallas, M. R.; Chu Y. C.; Piermarini, G. J. *J. Mater. Res.* **1995**, *10*, 2817.

(6) Nelson, D. F.; Sturge, M. D. *Phys. Rev.* **1965**, *137*, 1117.

(7) Lee, K. H.; Crawford, J. H. *Phys. Rev. B* **1979**, *19*, 3217.

(8) Brewer, J. D.; Jeffries, B. T.; Summers, G. P. *Phys. Rev. B* **1980**, *22*, 4900.

(9) Carrasco, J.; Lopez, N.; Sousa, C.; Illas, F. *Phys. Rev. B* **2005**, *72*, 054109.

(10) Xu, Y.; Gu, Z.; Zhong, X.; Ching, W. Y. *Phys. Rev. B* **1997**, *56*, 7277.

(11) Draeger, B. G.; Summers, G. P. *Phys. Rev. B* **1979**, *19*, 1172.

(12) Ma, Q.; Clarke, D. R. *J. Am. Ceram. Soc.* **1993**, *76*, 1433.

(13) Zhu, W.; Wan, K.; Pezzotti, G. *Meas. Sci. Technol.* **2006**, *17*, 191.

(14) Porto, S. P. S.; Krishnan, R. S. *J. Chem. Phys.* **1967**, *47*, 1009.

(15) Kadleíková, M.; Breza, J.; Veselý, M. *Microelectron. J.* **2001**, *32*, 955.

(16) Pezzotti, G.; Wan, K.; Munisso, M. C.; Zhu, W.; *Appl. Phys. Lett.* **2006**, *89*, 041908.

(17) Grabner, L. *J. Appl. Phys.* **1978**, *49*, 580.

(18) Roedel, J.; Seidel, J. *J. Am. Ceram. Soc.* **1997**, *80*, 433.

(19) Zhu, W.; Pezzotti, G. *Appl. Spectrosc.* **2005**, *59*, 1042.

(20) Fett, T. Forschungszentrum Karlsruhe Report No. FZKA 6757, 2002.

(21) Kanaya, K.; Okayama, S. *J. Phys. D: Appl. Phys.* **1972**, *5*, 43.

(22) Lee, K. H.; Crawford, J. H. *Appl. Phys. Lett.* **1978**, *33*, 273.

(23) Caulfield, K. J.; Cooper, R. *Phys. Rev. B* **1993**, *47*, 55.

(24) Srudp, A. I.; Kortov, V. S.; Pustovarov, V. A.; Yakovelev, V. Y. *Phys. Status Solidi C* **2005**, *2*, 527.

(25) http://global.Kyocera.com/prdct/fc/product/material/sap/, accessed May 4, 2006.

(26) Porporati, A. A.; Tanaka, Y.; Matsutani, A.; Zhu, W.; Pezzotti, G. *J. Appl. Phys.* **2006**, *100*, 083515.

(27) Pezzotti, G.; Zhu, W.; Leto, A.; Matsutani, A.; Porporati, A. A. *J. Phys. D: Appl. Phys.* **2006**, *39*, 4975.

(28) Zhu, W.; Porporati, A. A.; Matsutani, A.; Lama, N.; Pezzotti, G. *J. Appl. Phys.* in press.

(29) Broek, D. Elementary engineering fracture mechanics, Martinus Nijhoff: New York, 1982; Chapter X.

(30) Yoffe, E. H. *Philos. Mag. A* **1982**, *46*, 617.

(31) Saito, H.; Taguchi, M.; Ohishi, M.; Yoneta, M.; Imai, K. *Phys. Status Solidi C* **2004**, *1*, 2478.

(32) Hickernell, F. S. *Sonics and Ultrasonics* **1985**, *32*, 621.

(33) Shen, Z. Y.; Wilker, C.; Pang, P.; Holstein, W. L.; Face, D.; Kountz, D. J. *Microwave Theory and Techniques* **1992**, *40*, 2424.

(34) Lindmayer, M.; Mosebach, H. *Appl. Supercond.* **1999**, *9*, 1369.

(35) Hirayama, H.; Kyono, T.; Akita, K.; Nakamura, T.; Ishibashi, K. *Phys. Status Solidi C* **2005**, *2*, 2899.